

Fermi surface properties of AB_3 (A = Y, La; B = Pb, In, Tl) intermetallic compounds under pressure

This article has been downloaded from IOPscience. Please scroll down to see the full text article.

2013 J. Phys.: Condens. Matter 25 155501

(<http://iopscience.iop.org/0953-8984/25/15/155501>)

View [the table of contents for this issue](#), or go to the [journal homepage](#) for more

Download details:

IP Address: 218.248.6.153

The article was downloaded on 02/04/2013 at 09:36

Please note that [terms and conditions apply](#).

Fermi surface properties of AB_3 ($A = Y, La$; $B = Pb, In, Tl$) intermetallic compounds under pressure

Swetarekha Ram¹, V Kanchana¹, A Svane², S B Dugdale³ and N E Christensen²

¹ Department of Physics, Indian Institute of Technology Hyderabad, Ordnance Factory Estate, Yeddumailaram-502 205, Andhra Pradesh, India

² Department of Physics and Astronomy, Aarhus University, DK-8000 Aarhus C, Denmark

³ H H Wills Physics Laboratory, University of Bristol, Tyndall Avenue, Bristol BS8 1TL, UK

E-mail: kanchana@iith.ac.in

Received 14 January 2013, in final form 6 March 2013

Published 25 March 2013

Online at stacks.iop.org/JPhysCM/25/155501

Abstract

The electronic structures, densities of states, Fermi surfaces and elastic properties of AB_3 ($A = La, Y$; $B = Pb, In, Tl$) compounds are studied under pressure using the full-potential linear augmented plane wave (FP-LAPW) method within the local density approximation for the exchange–correlation functional and including spin–orbit coupling. Fermi surface topology changes are found for all the isostructural AB_3 compounds under compression (at $V/V_0 = 0.90$ for $LaPb_3$ (pressure = 8 GPa), at $V/V_0 = 0.98$ for $AlIn_3$ (pressure = 1.5 GPa), at $V/V_0 = 0.80$ for ATl_3 (pressure in excess of 18 GPa)) apart from YPb_3 , although its electronic structure at zero pressure is very similar to that of $LaPb_3$. For $LaPb_3$ a softening of the C_{44} elastic constant under pressure (equivalent to 8 GPa) may be related to the appearance of a new hole pocket around the X point. From the calculated elastic properties and other mechanical properties, all the compounds investigated are found to be ductile in nature with elastic anisotropy. The states at the Fermi level (E_F) are dominated by B p states with significant contributions from the A d states. For the La compounds, small hybridizations of the La f states also occur around E_F .

(Some figures may appear in colour only in the online journal)

1. Introduction

Intermetallic compounds of the form AB_3 (where A is a rare earth element or Y, and B is In, Sn, Tl or Pb) crystallizing in the $AuCu_3$ type structure with space group $Pm\bar{3}m(221)$ have attracted great interest because of their oscillatory superconducting properties, magnetic susceptibility and thermopower, as functions of their valence electron concentration [1–3]. Recently Bittar *et al* [4] found that the effective exchange interaction parameter decreases upon substitution of Sn in $LaIn_{3-x}Sn_x$ alloy and suggested that this is due to the increase of the lattice parameter. Canepa *et al* [5] explained the anomalous behaviour of the heat capacity at constant volume (C_V) for $LaPb_3$ with temperature

in terms of the presence of anharmonic lattice vibrations. Recently the superconducting transition temperature (T_c) of $LaIn_3$ has been reported to be 1.08 K, 0.95 K and 0.9 K from resistivity, susceptibility and heat capacity measurements, respectively [6]. To understand and explore the different properties of AB_3 intermetallic compounds, we have examined the electronic structure of AB_3 ($A = La, Y$ and $B = In, Tl, Pb$) at ambient as well as at high pressure and compared the findings with those of earlier studies of $LaSn_3$ and YSn_3 [7, 8]. The main aim of this paper is to study the Fermi surface (FS) topology under pressure, which might help us to understand the superconducting properties of these compounds. A FS topology change was reported for the isostructural Kondo lattice compound $CeIn_3$ [9, 10]

Table 1. Calculated lattice constants a (in Å) and bulk moduli B (in GPa) for AB_3 ($A = \text{La, Y}$; $B = \text{Pb, In, Tl}$), as obtained with the LDA approximations for exchange and correlation. The bulk moduli are evaluated at the theoretical equilibrium volumes. Experimental values are quoted for comparison. The experimental lattice constants which we have used in our present calculation for LaPb_3 , LaIn_3 , LaTl_3 , YPb_3 , YIn_3 , and YTl_3 are 4.903 Å, 4.725 Å, 4.799 Å, 4.813 Å, 4.592 Å and 4.678 Å respectively.

Compounds		Lattice constants	B
LaPb_3	Present work	4.838	62
	Experiment	4.903 ^a , 4.905 ^b	
LaIn_3	Present work	4.66	64
	Other theory	4.70 ^c , 4.925 ^d	
	Experiment	4.739 ^b , 4.725 ^e , 4.735 ^f	
LaTl_3	Present work	4.747	62
	Experiment	4.806 ^a , 4.799 ^b	
YPb_3	Present work	4.76	63
	Experiment	4.813 ^b , 4.823 ^f	
YIn_3	Present work	4.514	70
	Experiment	4.592 ^b , 4.594 ^f , 4.593 ^g	
YTl_3	Present work	4.615	66
	Experiment	4.678 ^b , 4.68 ^f	

^a Reference [26]. ^b Reference [1]. ^c LMTO-ASA; reference [14].

^d ASW; reference [15]. ^e Reference [28]. ^f Reference [29].

^g Reference [12].

which is antiferromagnetic with $T_N = 10$ K and exhibits superconductivity below 0.2 K under 2.5–2.7 GPa pressure. The de Haas–van Alphen effect was studied for LaIn_3 [11], YIn_3 [12] and antiferromagnetic GdIn_3 [13]. A few theoretical studies of the electronic structure of LaIn_3 [14–16] are also available. Many studies on the physical properties of LaB_3 ($B = \text{In, Tl, Sn, Pb}$) and their alloys have been reported earlier [2, 3, 17–19], but no theoretical study comparing the electronic structures of AB_3 ($A = \text{La, Y}$ and $B = \text{In, Tl, Pb}$) at ambient or at high pressure is available. In the present work, the energy band structure, density of states, Fermi surface, elastic constants and mechanical properties at ambient conditions as well as under pressure are calculated. A FS topology change is found in all the AB_3 compounds investigated apart from YPb_3 , and analysed using the respective band structures. The remainder of this paper is organized as follows. In section 2, the computational details are described. Section 3 presents the results and discussions of these. Section 4 contains a brief summary and the conclusions.

2. The method of calculation

First-principles calculations were performed using the full-potential linear augmented plane wave (FP-LAPW) method [20] as implemented in the WIEN2k [21] code. For the exchange–correlation functional the local density approximation (LDA) in the form proposed by Perdew and Wang [22] was used. For the energy convergence, the criterion $R_{\text{MT}}K_{\text{max}} = 8$ was used, where R_{MT} is the smallest muffin-tin radius, and K_{max} is the plane wave cut-off. The charge density was Fourier expanded up to $G_{\text{max}} = 9$ (au^{-1}). We carried out convergence tests for the charge-density Fourier expansion using higher G_{max} values and found no significant changes in the calculated properties. The muffin-tin radii were chosen as 2.95 bohr for both La and Y and 2.85 bohr for the B atoms. A $32 \times 32 \times 32$ k -point mesh in the Monkhorst–Pack [23] scheme

was used during the self-consistency cycle. The total energy was converged to 10^{-6} Ryd. The Birch–Murnaghan equation of state [24] was used to fit the total energy as a function of unit cell volume to obtain the equilibrium lattice constants and bulk moduli for the systems investigated. A $44 \times 44 \times 44$ mesh, which corresponds to 2300 k -points in the irreducible part of the Brillouin zone (BZ), was used for the Fermi surface calculations to ensure accurate determination of the Fermi level. The three-dimensional Fermi surface plots were generated with the help of the Xcrysden molecular structure visualization program [25]. Spin–orbit coupling (SOC) was included in all the electronic structure calculations.

3. Results and discussion

3.1. Ground-state properties

The calculated equilibrium lattice parameters a and zero-pressure bulk moduli B are listed in table 1. The results are in good agreement with available experimental data and other calculations. The lattice constants are slightly underestimated with respect to their experimental values, between 1.1% (for LaTl_3) and 1.7% (for YIn_3), a well-known deficiency of the LDA. No experimental results are available for the bulk moduli. The calculated bulk moduli for all compounds are very similar, between 62 and 70 GPa. This also holds for the LaSn_3 and YSn_3 compounds, for which LDA calculations gave $B = 68$ GPa and 71 GPa, respectively [7].

3.2. The band structure and density of states

Figure 1 shows the band dispersions along the high symmetry directions together with the density of states (DOS) of the series of AB_3 compounds at experimental volume (V_0). Our calculated band structure of LaIn_3 is similar to that of [14]. Comparing the band structures of all the AB_3 compounds

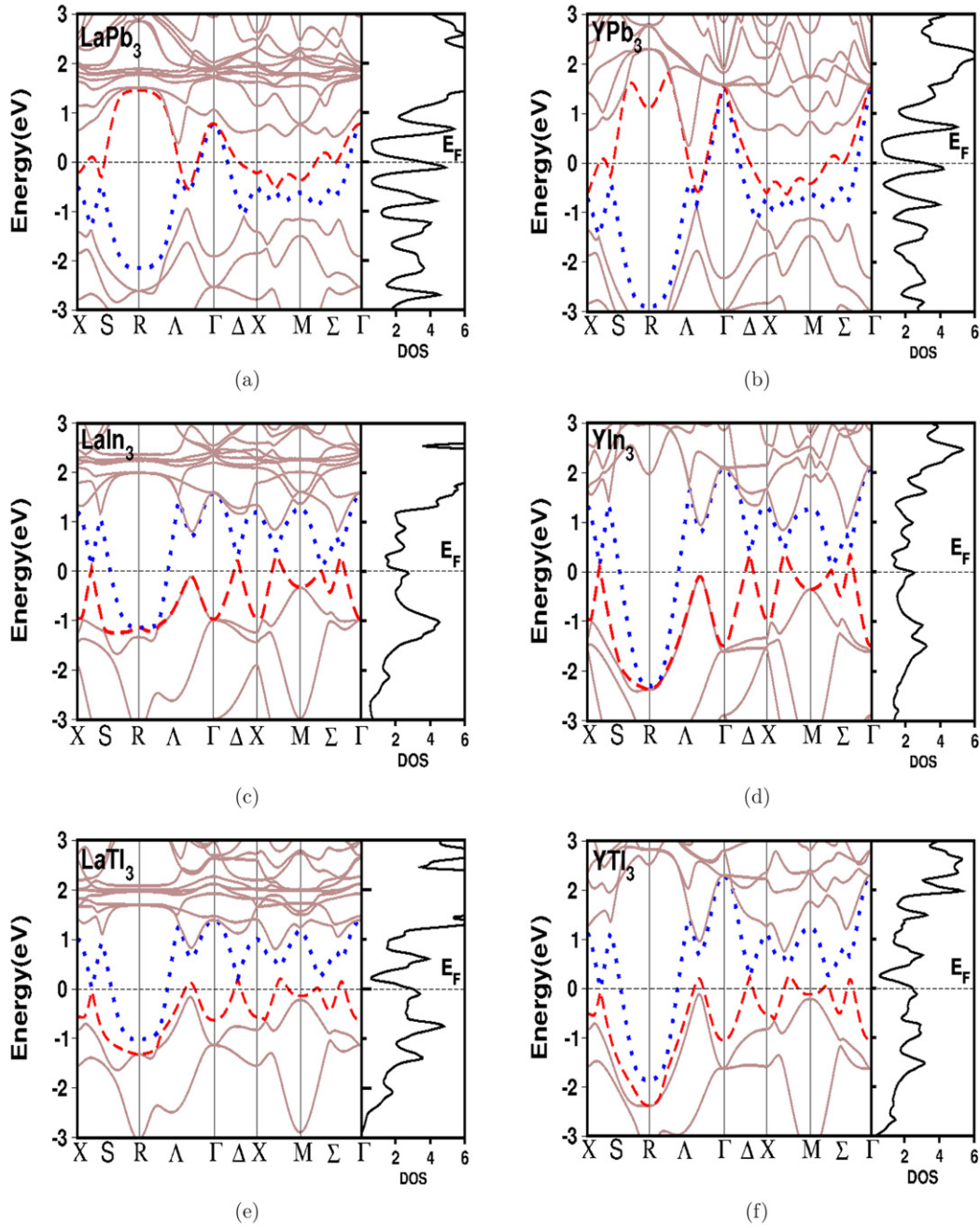


Figure 1. Band structure and density of states of AB_3 ($A = \text{La, Y}$; $B = \text{Pb, In, Tl}$) compounds at their experimental lattice constants. Two bands cross the Fermi level, marked in the plots by a red dashed line and a blue dotted line. The unit of the DOS is states per eV per formula unit.

investigated for $A = \text{La, Y}$ and $B = \text{Pb, In, Tl}$, it is evident that the bands in the vicinity of the Fermi level for LaB_3 and YB_3 look very similar along all the high symmetry lines at zero pressure. In contrast, the electronic structures of LaSn_3 and YSn_3 [7, 8] did display some discrepancies around E_F , particularly in the regions close to the X and M points in the Brillouin zone. On the other hand, when comparing the electronic structures of the AB_3 compounds with the same A but varying B, some minor deviations are seen. For $B = \text{Sn, Pb}$, which corresponds to an average valence electron count (number of valence electrons per atom) of $n = 3.75$, slight differences around the X and M points are evident from

comparison of the band structures in figures 1(a) and (b) for the Pb compounds with their Sn counterparts in [7]. For $B = \text{In, Tl}$, having valence electron count $n = 3$, deviations in the band structure along the Λ and S symmetry lines are observed, in figures 1(c)+(e) for $A = \text{La}$ and in figures 1(d)+(f) for $A = \text{Y}$. For AlIn_3 , in figures 1(c) and (d), the band marked in red crosses E_F twice along the S line but not along Λ . In contrast, for ATl_3 the same (red coloured, broken line) band in figures 1(e) and (f) does not cross E_F along S, but crosses twice along Λ .

These minor differences lead to slight differences also in the Fermi surfaces of the AB_3 compounds, which are

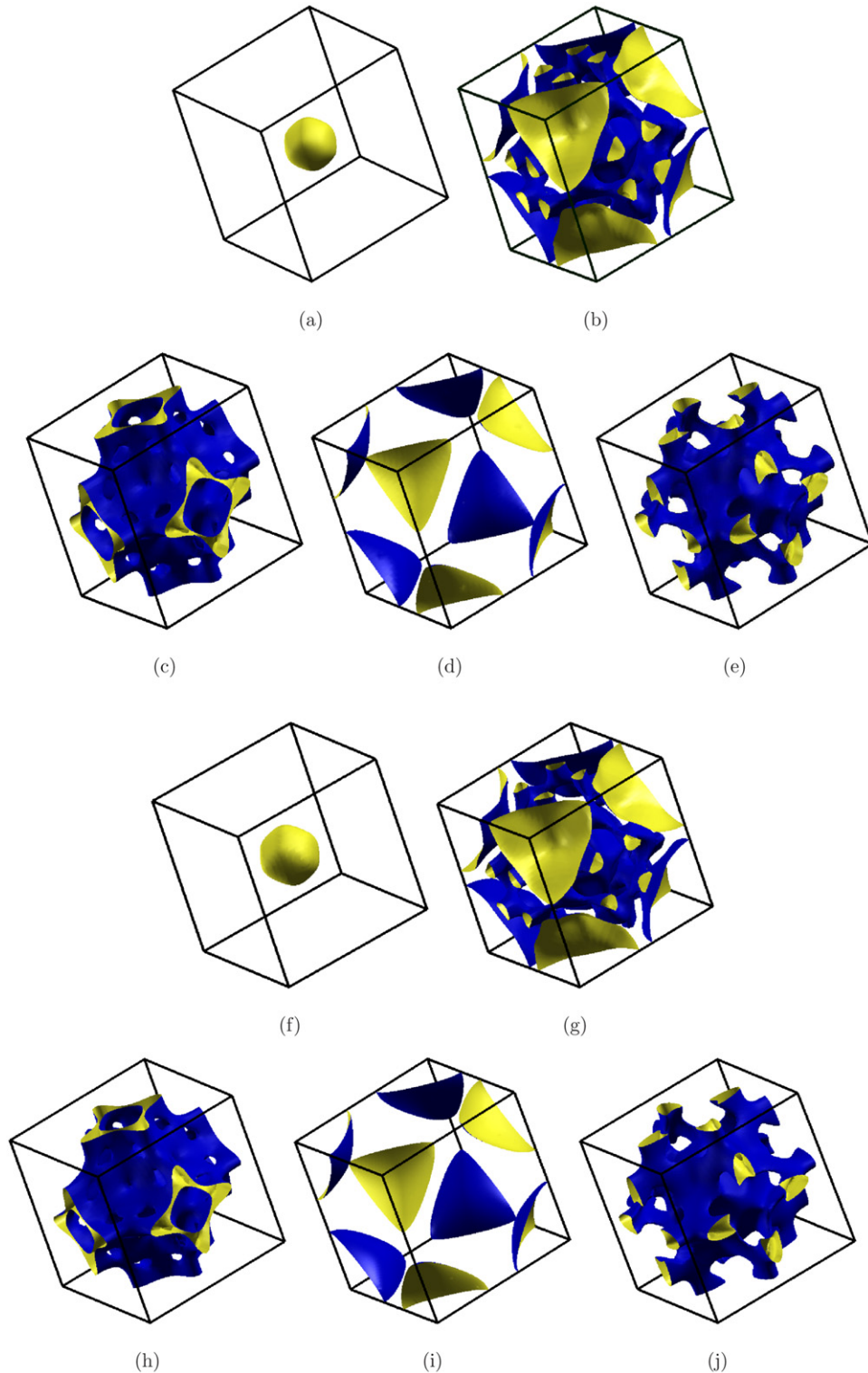


Figure 2. Fermi surface at zero pressure of: LaPb_3 ((a), (b)); LaIn_3 ((c), (d)); LaTl_3 (e); YPb_3 ((f), (g)); YIn_3 ((h), (i)); and YTl_3 (j), at experimental lattice constants. The topology of the Fermi surface of LaB_3 is similar to that of YB_3 for $B = \text{Pb, In, Tl}$. The topology of the first sheet for APb_3 is similar to that of its ASn_3 counterpart (not shown). Similarly, the topology of the second sheet for AlIn_3 is similar to that of its ATl_3 counterpart, which is not shown. The colour coding is such that yellow (blue) faces towards regions of the Brillouin zone with unoccupied (occupied) states.

displayed in figures 2(a)–(j). In all cases two Fermi surface sheets are observed, with the exception of that of YSn_3 , for which a small third surface exists [7]. For the $B = \text{In}$ or Tl

compounds, the first sheet is rather complex, while the second sheet is simpler: an electron surface centred around the R point. Thus, the second sheets of the ATl_3 compounds are

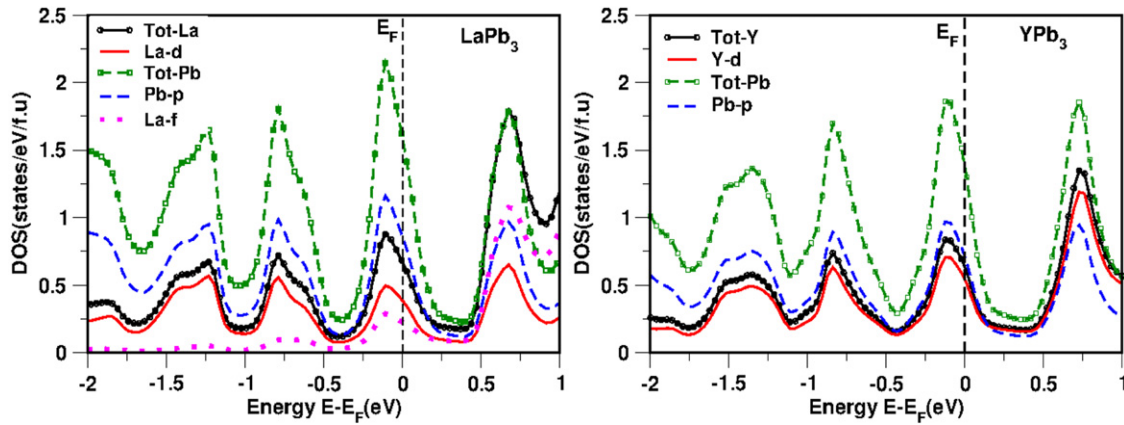


Figure 3. Partial densities of states of APb_3 in the vicinity of the Fermi level. The densities of states are decomposed into their weights per A and B atom, and for $A = La$ also on the La f orbitals. The Pb p part contributes the most to the density of states at E_F ; however the A d part of the hybridization is significant. The total A and B contributions are about equal at E_F . The unit of the DOS is states per eV per formula unit.

very similar to the second sheets of their In homologues, so only the latter are shown in figures 2(d) and (i). Similarly, for the $n = 3.75$ compounds with $B = Sn$ or Pb , the first Fermi sheet is a simple almost-spherical hole surface centred on the Γ point, while the second sheet is complex. The first surfaces of the Pb compounds are included in figures 2(a) and (f), while the Sn cases were shown in [7]. As for the topologies of the complex Fermi sheets, one observe very close similarity between the LaB_3 and YB_3 homologous compounds: compare figures 2(b)–(g) for $B = Pb$, figures 2(c)–(h) for $B = In$, and figures 2(e)–(j) for $B = Tl$. As mentioned, for the Sn compounds some small differences are seen [7]. A distinct difference between La and Y is the proximity of the f levels of La to the Fermi energy (figure 1), which introduces f hybridization into the states around the Fermi level in the La compounds, which is not present in the Y compounds. The similarity between the Fermi surfaces of the La and Y compounds shows that this f hybridization into the bands around the Fermi level is rather insignificant. From the partial densities of states, exemplified for $LaPb_3$ and YPb_3 in figure 3, the La d states are seen to have larger weight at E_F than the La f states. In contrast, for $LaSn_3$ the La f state contribution to the density of states at the Fermi level was found to be relatively large [7], which in combination with the SOC leads to the slight differences in band structure between $LaSn_3$ and YSn_3 . For the present AB_3 compounds, B being In, Tl or Pb, the effects of SOC are very similar in the La and Y homologues.

Looking next at the Fermi surfaces of AB_3 compounds for the same element A, we find larger differences for the complex Fermi sheet depending on the B element. Thus, comparing $LaSn_3$ [7] and $LaPb_3$ (figure 2(b)), the connectivities on the faces of the cubic Brillouin zone (which include points X and M) differ. Similar conclusions are reached for $LaIn_3$ and $LaTl_3$ (figures 2(c) and (e)) as well as for YIn_3 and YTl_3 (figures 2(h) and (j)). For YSn_3 [7, 8] and YPb_3 , figure 2(g), the connectivity in the vicinity of the M points (i.e. the middles of the cube edges) is different, with a detached electron pocket in the former case. The feature is

relatively robust, being common to that list of compounds, and insensitive to the choice of exchange–correlation functional.

The densities of states are included in figure 1. In all the AB_3 compounds, we find strong hybridization between the B p states and the A d states in the region around the Fermi level. This is illustrated for $LaPb_3$ and YPb_3 in figure 3. At E_F , the total A and B contributions (per atom) are about equal. The La f bands contribute a large density of states around 2 eV above the Fermi level in the LaB_3 compounds, which naturally is absent in the YB_3 homologues (see figure 1), but in the vicinity of E_F the DOS looks quite similar, i.e. no particular effect of f hybridization influences the DOS at E_F . In the Pb compounds, distinct pseudogaps appear both above and below E_F as shown in figures 1(a)–(b) and 3(a)–(b). In the Tl compounds, a pseudogap appears only above E_F , while no particular features appear around E_F for the In compounds, which is also evident from figures 1(c)–(f). Interestingly, the Sn compounds reveal a pseudogap only below E_F [8], so we may rationalize such that the pseudogap above E_F is a feature associated with the heavier B elements Tl and Pb, while the pseudogap below E_F is a feature of the $n = 3.75$ compounds with $B = Sn, Pb$.

The evolution of the total density of states at the Fermi level for the AB_3 compounds under compression is shown in figure 4. The behaviour is largely monotonically decreasing, with minor irregularities, which may be related to Fermi surface topology changes under compression, to be discussed in section 3.3.

3.3. The Fermi surface topology under pressure

In all AB_3 compounds studied in the present work there are two sheets of the Fermi surface corresponding to the two bands crossing the Fermi level in figure 1 (dashed line (red) and dotted line (blue)). The Fermi surfaces are shown in figure 2. One of the two surfaces is the complicated surface (figures 2(b)–(c), (e)) and the other surface consists of a hole pocket centred at the Γ point for AB_3 with $B = Sn, Pb$ as shown in figure 2(a) and it is an electron pocket around the

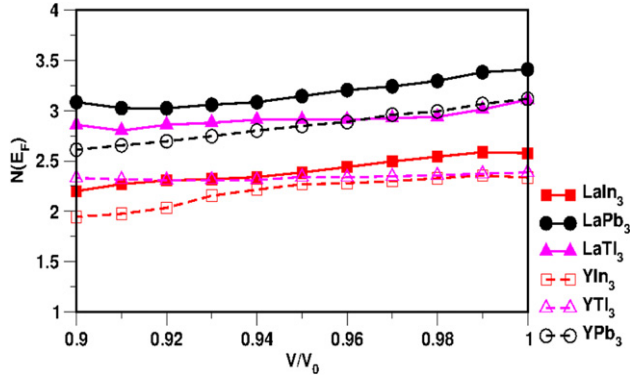


Figure 4. Variation of the densities of states at the Fermi level, $N(E_F)$, under compression for AB_3 ($A = \text{La, Y}$; $B = \text{Pb, In, Tl}$). The unit of the density of states is states per eV per formula unit.

R point in the Brillouin zone for $B = \text{In, Tl}$ as shown in figure 2(d) at zero pressure. The topology of the Fermi surface of LaB_3 is found to be similar to that of YB_3 for $B = \text{Pb, In, Tl}$ at ambient pressure, as shown in figure 2, which again illustrates the dominating nature of the B p-like states in the vicinity of the Fermi level. But the topology of YSn_3 is slightly different, where (at ambient pressure) it has an extra electron pocket along the Δ line, which for LaSn_3 [7] only appears under pressure. As we discussed earlier, the differences among Pb and Sn containing compounds are seen particularly at the X and M points in the BZ, as can be seen from the complicated Fermi surfaces in figures 2(b), (g) for Pb containing compounds and in [7, 8] for Sn containing compounds. It is interesting to note that the topologies of the Fermi surfaces of the Sn, Pb containing compounds are completely different from the topologies of In, Tl containing compounds. Now, when we compare Aln_3 with ATl_3 , we observe the very similar electronic structures in the vicinity of the Fermi level, except for points along the Δ and S symmetry lines as discussed earlier, resulting in the hollow triangular tubes interconnected along the S line in Aln_3 (see figures 2(c) and (h)) and an open gap is not seen along the Δ line in ATl_3 (see figures 2(e) and (j)). Our calculated FS of LaIn_3 is also quite similar to that from the earlier study [11]. Apart from

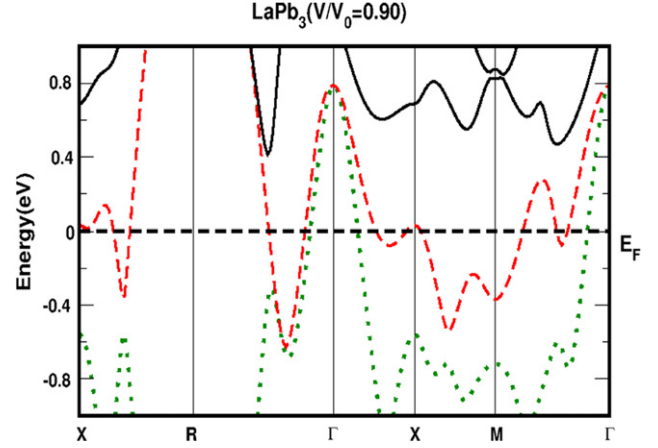


Figure 6. Band structure of LaPb_3 at $V/V_0 = 0.90$. A new hole pocket is emerging at the X point.

this, we find the Fermi surface topologies of LaIn_3 and YIn_3 to be the same at zero pressure, as is also evident from the band structure plots in figure 1. This contradicts the experimental results of Pluzhnikov *et al* [12], who found a new branch in the dHvA frequencies of YIn_3 for magnetic field directions near $\langle 100 \rangle$ with no counterpart in LaIn_3 .

Under compression, Fermi surface topology changes are found in all the compounds apart from YPb_3 . In LaPb_3 a new hole pocket appears at the X point for a compression $V/V_0 = 0.90$ (corresponding to an applied pressure around 8 GPa), as shown in figure 5(a). This is also seen from the band structure plot in figure 6. This is mainly due to the upward movement of the band only at the X point, irrespective of the other points in the BZ, where the simultaneous downward shift of the band is found under pressure. In our previous study, the same hole pocket is also found in LaSn_3 at ambient pressure. But no such topology change is seen in YPb_3 , like for YSn_3 , although they have the same band structure as LaPb_3 around E_F at ambient pressure (see figures 1(a) and (b)). This could be due to the band being more dispersive in YPb_3 , especially at the X point, as can be seen in figure 1(b) (red, dashed line), and of Y d character at that particular point. Under pressure, the FS topologies of LaSn_3 and LaPb_3

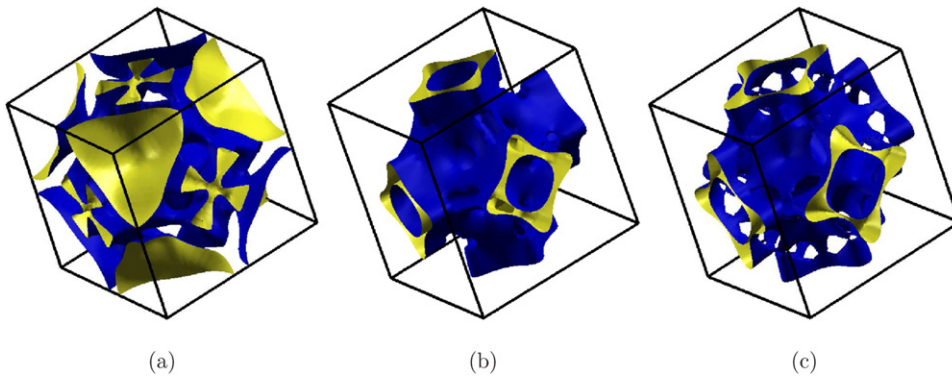


Figure 5. Fermi surface of: LaPb_3 at $V/V_0 = 0.90$ (a); LaIn_3 at $V/V_0 = 0.98$ (b); LaTl_3 at $V/V_0 = 0.80$ (c). V_0 refers to the experimental equilibrium volume.

Table 2. Elastic constants and derived quantities for AB₃, as calculated with LDA at the theoretical equilibrium volume. *A* is the anisotropy factor ($A = 2C_{44}/(C_{11} - C_{12})$) and $C_p = C_{12} - C_{44}$ is the Cauchy pressure.

Parameters	LaPb ₃	LaIn ₃	LaTl ₃	YPb ₃	YIn ₃	YTl ₃
C_{11} (GPa)	83.5	103.9	90.6	70.0	106.2	93.0
C_{12} (GPa)	50.5	44.5	46.4	59.5	48.7	53.6
C_{44} (GPa)	35.8	37.7	31.6	28.0	33.6	30.4
<i>A</i>	2.17	1.27	1.43	5.3	1.17	1.54
G_H (GPa)	26.2	34.3	27.4	14.6	31.6	25.6
<i>E</i> (GPa)	68.9	87.3	71.5	40.7	81.9	68.0
σ	0.31	0.27	0.30	0.39	0.30	0.33
G_H/B	0.43	0.53	0.45	0.23	0.46	0.38
C_p (GPa)	14.7	6.8	14.7	31.5	15.1	23.2
v_l (km s ⁻¹)	2.94	3.72	2.89	2.75	3.75	2.92
v_t (km s ⁻¹)	1.53	2.08	1.53	1.16	2.0	1.47
Θ_D (K)	167.6	234.80	170.5	129.8	234.9	168.7
	147 ^a	170 ^a , 194.4 ^b				

^a Reference [27].^b Reference [30]. (Experiment: from specific heat measurements.)

are nearly identical, and this indicates that LaPb₃ and LaSn₃ could behave alike under compression. As noted by Havinga *et al* [1], the variation of T_c is quite regular for La(Pb_{1-x}Sn_x)₃ alloys without changing the valence electron concentration, which may also support our result. The FS topology remains unchanged for the other simple hole pocket (see figures 2(a) and (f), and the blue colour, dotted line band in figures 1(a) and (b)) under compression. Comparing AlIn₃ and AlTl₃ under compression near $V/V_0 = 0.98$ (pressure around 1.5 GPa) a FS topology change is observed in AlIn₃ due to a downward shift of the band along the Σ line which is mainly of In p character, resulting in the interconnected triangular open tubes becoming disconnected along the same Σ line, as is evident from figure 5(b). In the case of AlTl₃ a FS topology change is found near $V/V_0 = 0.80$ (corresponding to a pressure in excess of 18 GPa) and is illustrated in figure 5(c). Under compression, the downward shift of the band is seen along the Σ line, as in AlIn₃, with a simultaneous upward movement of the band along the S line. Owing to this, the triangular open regions open up along S, with simultaneous partial detachment of the same open tube along Σ , and the band character is mainly Tl p like. The same simultaneous upward shift of the band is also observed in AlIn₃ along S, but it does not alter the vicinity of E_F in that particular direction. Under compression, the FS topology of AlTl₃ is quite similar to that of AlIn₃. The topology of the second surface remains the same for all In and Tl containing compounds at ambient as well as at higher compressions (see figures 2(d) and (i), and the blue colour dotted line band in figures 1(c)–(f)). Under compression, the topology of LaPb₃ looks like that of LaSn₃, and similarly the topology of AlIn₃ looks like that of AlTl₃.

3.4. Elastic constants and mechanical properties

The elastic constants have been calculated within the total-energy method; see table 2. A cubic crystal has only three independent elastic constants [31, 32]: C_{11} , C_{12} and C_{44} . To the best of our knowledge, no experimental values of the elastic constants of these compounds have been reported to

date. All the compounds investigated are mechanically stable and satisfy the stability criteria for the cubic system, i.e. $C_{11} > C_{12}$, $C_{44} > 0$, and $C_{11} + 2C_{12} > 0$. From these, one may obtain Hill's [33] shear modulus G_H (which is the arithmetic mean of the Reuss [34] and Voigt [35] approximations). Apart from this, there is no structural phase transition known in the pressure range studied for all the compounds investigated here, which is further confirmed from the phonon spectrum and is yet to be published. All the compounds are found to be ductile in nature according to Pugh's criterion [36]: $G_H/B < 0.57$, as seen from the values of G_H/B in table 2. Cauchy's pressure ($C_p = C_{12} - C_{44}$) is another index for determining the ductile/brittle nature of metallic compounds, where positive (negative) values correspond to ductile (brittle) materials. The calculated Cauchy pressures for the compounds considered here are all positive, i.e. also indicating a ductile nature. Poisson's ratio σ (see table 2) is another important parameter for describing the ductile nature of solids. σ is typically around 0.33 [37] for the ductile materials. Thus from the calculated values of σ , the ductility of these compounds is again confirmed. Another important parameter is the elastic anisotropy factor, *A*, which gives a measure of the anisotropy in the crystal. For isotropic crystals, $A = 1$, while values smaller or greater than unity measure the degree of elastic anisotropy. All of the compounds investigated here are elastically anisotropic in nature, with YPb₃ being the most anisotropic among all the compounds, as seen from table 2. Having calculated Young's modulus *E*, the bulk modulus *B*, and the shear modulus *G*, one may derive the Debye temperature using the equation

$$\Theta_D = \frac{h}{k_B} \left(\frac{3n\rho N_A}{4\pi M} \right)^{1/3} v_m, \quad (1)$$

where *h*, k_B and N_A are Planck's and Boltzmann's constants, and Avogadro's number, respectively. ρ is the mass density, *M* the molecular weight, and *n* the number of atoms in the unit cell. The mean sound velocity is defined as

$$v_m = \left[\frac{1}{3} \left(\frac{2}{v_t^3} + \frac{1}{v_l^3} \right) \right]^{-1/3}, \quad (2)$$

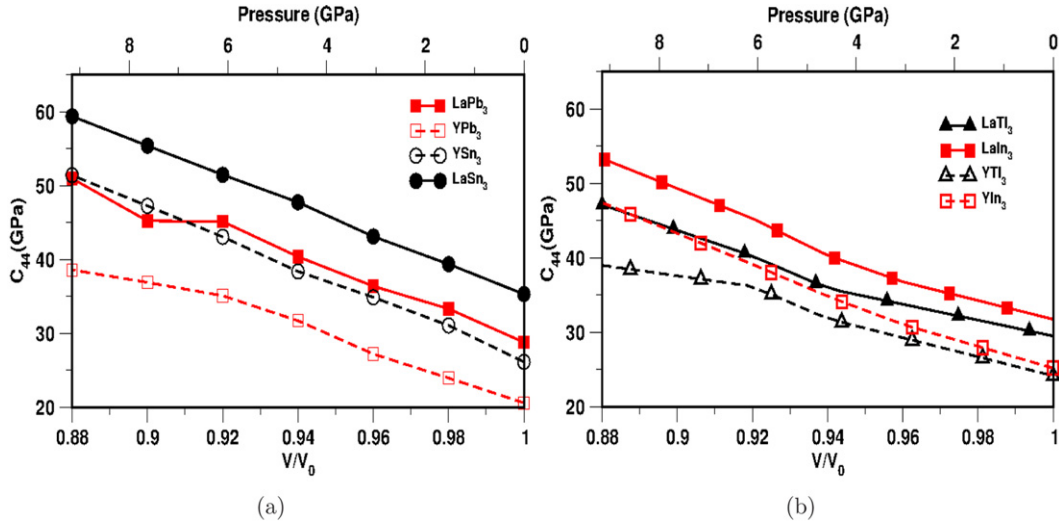


Figure 7. Variation of the C_{44} elastic constant with compression in AB_3 compounds, with $A = La, Y$ and: (a) $B = Sn, Pb$; (b) $B = In, Tl$. An approximate pressure scale is added at the top, based on an average bulk modulus $B = 65$ GPa for the family of compounds considered (see table 1).

where v_l and v_t are the longitudinal and transverse sound velocities, which may be obtained from the shear modulus G_H and bulk modulus B using

$$v_l = \sqrt{\frac{\left(B + \frac{4}{3}G_H\right)}{\rho}} \quad (3)$$

and

$$v_t = \sqrt{\frac{G_H}{\rho}}. \quad (4)$$

We also calculated the elastic constants for the AB_3 compounds under compression, as shown in figure 7. An elastic softening is found in C_{44} for $LaPb_3$ near $V/V_0 = 0.9$ (pressure around 8 GPa). This might be related to the new hole pocket appearing at the X point at this compression of $LaPb_3$.

4. Conclusion

The Fermi surface topology change under compression is observed for all the isostructural compounds AB_3 investigated ($A = La, Y$; $B = Pb, In, Tl$) except YPb_3 . The calculated elastic constants and the related mechanical properties confirmed the ductility of all the AB_3 compounds. In addition we found an elastic softening of C_{44} under pressure only in $LaPb_3$, which might be related to the appearance of a new hole pocket at the X point. The FS topology change observed in other compounds is different from that in $LaPb_3$, namely slight reconstructions of the complicated FS sheet. The similar band structures, densities of states and Fermi surfaces along with the nearly identical T_c values under ambient conditions for La and Y containing compounds with particular B atoms indicate the dominant nature of the B p character as discussed by Toxen *et al* [2]. However, a close analysis of the superconductive properties of the AB_3 compounds examined here, including possible relations to

Fermi surface topologies and their variations with applied pressure, require further studies, including calculations of electron–phonon interactions and of T_c . This work has been initiated, and the results will be reported later [38].

Acknowledgments

SR and VK acknowledge IIT Hyderabad for the High Performance Computing (HPC) facility. SR acknowledges IIT Hyderabad for the Research Fellowship.

References

- [1] Havinga E E, Damsma H and Van Maaren M H 1970 *J. Phys. Chem. Solids* **31** 2653
- [2] Toxen A M, Gambino R J and Welsh L B 1973 *Phys. Rev. B* **8** 90
- [3] Toxen A M and Gambino R J 1968 *Phys. Lett. A* **28** 214
- [4] Bittar E M, Adriano C, Giles C, Rettori C, Fisk Z and Pagliuso P G 2011 *J. Phys.: Condens. Matter* **23** 455701
- [5] Canepa F, Costa G A and Olcese G L 1983 *Solid State Commun.* **45** 725
- [6] Johnson S D, Young J R, Zieve R J and Cooley J C 2012 *Solid State Commun.* **152** 513
- [7] Ram S, Kanchana V, Vaitheeswaran G, Svane A, Dugdale S B and Christensen N E 2012 *Phys. Rev. B* **85** 174531
- [8] Dugdale S B 2011 *Phys. Rev. B* **83** 012502
- [9] Settai R, Kubo T, Shishido H, Kobayashi T C and Ōnuki Y 2004 *J. Magn. Magn. Mater.* **272–276** 223
- [10] Mathur N D, Grosche F M, Julian S R, Walker I R, Freye D M, Haselwimmer R K W and Lonzarich G G 1998 *Nature* **394** 39
- [11] Kitazawa H, Gao Q Z, Shida H, Suzuki T, Hasegawa A and Kasuya T 1985 *J. Magn. Magn. Mater.* **52** 286
- [12] Pluzhnikov V B, Czopnik A and Svechekarev I V 1995 *Physica B* **212** 375
- [13] Kletowski Z 2003 *Phys. Status Solidi a* **196** 356
- [14] Tang S-p, Zhang K-m and Xie X-d 1989 *J. Phys.: Condens. Matter* **1** 2677
- [15] Hackenbracht D and Kübler J 1979 *Z. Phys. B* **35** 27
- [16] Freeman A J and Koelling D D 1972 *J. Physique Coll.* **33** C3 57

- [17] Grobman W D 1972 *Phys. Rev. B* **5** 2924
- [18] Havinga E E 1972 *Solid State Commun.* **11** 1249
- [19] Welsh L B, Toxen A M and Gambino R J 1972 *Phys. Rev. B* **6** 1677
- [20] Andersen O K 1975 *Phys. Rev. B* **12** 3060
- [21] Blaha P, Schwarz K, Madsen G K H, Kvasnicka D and Luitz J 2001 *WIEN2k, an Augmented Plane Wave + Local Orbitals Program for Calculating Crystal Properties* ed K Schwarz Techn. Universität Wien, Austria
- [22] Perdew J P and Wang Y 1992 *Phys. Rev. B* **45** 13244
- [23] Monkhorst H J and Pack J D 1976 *Phys. Rev. B* **13** 5188
- [24] Birch F 1947 *Phys. Rev.* **71** 809
- [25] Kokalj A 2003 *Comput. Mater. Sci.* **28** 155
- [26] Gambino R J, Stemple N R and Toxen A M 1968 *J. Phys. Chem. Solids* **29** 295
- [27] Kletowski Z, Fabrowski R, Sławiński P and Henkie Z 1997 *J. Magn. Magn. Mater.* **166** 361
- [28] Schwartz G P and Shirley D A 1977 *Hyperfine Interact.* **3** 67
- [29] Pearson W B 1967 *Handbook of Lattice Spacings and Structures of Metals and Alloys* vol 2 (Oxford: Pergamon)
- [30] Nasu S, Van Diepen A M, Neumann H H and Craig R S 1971 *J. Phys. Chem. Solids* **32** 2773
- [31] Nye J F 1985 *Physical Properties of Crystals: their Representation by Tensors and Matrices* (Oxford: Oxford University Press)
- [32] Mattesini M, Ahuja R and Johansson B 2003 *Phys. Rev. B* **68** 184108
- [33] Hill R 1952 *Proc. Phys. Soc. Lond. A* **65** 349
- [34] Reuss A 1929 *Z. Angew. Math. Mech.* **9** 49
- [35] Voigt W 1889 *Ann. Phys. Lpz.* **38** 573
- [36] Pugh S F 1954 *Phil. Mag.* **45** 823
- [37] Haines J, Leger J M and Bocquillon G 2001 *Annu. Rev. Mater. Res.* **31** 1
- [38] Ram S, Kanchana V, Vaitheeswaran G, Svane A, Dugdale S B and Christensen N E 2013 unpublished